Lab on a Chip

PAPER

View Article Online
View Journal

Cite this: DOI: 10.1039/c7lc00191f

A novel 3-D bio-microfluidic system mimicking *in vivo* heterogeneous tumour microstructures reveals complex tumour–stroma interactions†

Qihui Fan,[a] Ruchuan Liu,[b] Yang Jiao,[c] Chunxiu Tian,[d] James D. Farrell,[a] Wenwen Diao,[e] Xiaochen Wang,[a] Fengrong Zhang,[a] Wei Yuan,[f] Haibo Han,[g] Jinfeng Chen,[h] Yue Yang,[h] Xixiang Zhang,[d] Fangfu Ye,*[ai] Ming Li,[ai] Zhongcan Ouyang*[ei] and Liyu Liu*[b]

Received 24th February 2017,
Accepted 4th July 2017

DOI: 10.1039/c7lc00191f

rsc.li/loc

A 3-D microfluidic system consisting of microchamber arrays embedded in a collagen hydrogel with tuneable biochemical gradients that mimics the tumour microenvironment of mammary glands was constructed for the investigation on the interactions between invasive breast cancer cells and stromal cells. The hollow microchambers in collagen provide a very similar 3-D environment to that *in vivo* that regulates collective cellular dynamics and behaviour, while the microfluidic channels surrounding the collagen microchamber arrays allow one to impose complex concentration gradients of specific biological molecules or drugs. We found that breast epithelial cells (MCF-10A) seeded in the microchambers formed lumen-like structures similar to those in epithelial layers. When MCF-10A cells were co-cultured with invasive breast cancer cells (MDA-MB-231), the formation of lumen-like structures in the microchambers was inhibited, indicating the capability of cancer cells to disrupt the structures formed by surrounding cells for further invasion and metastasis. Subsequent mechanism studies showed that down regulation of E-cad expression due to MMPs produced by the cancer cells plays a dominant role in determining the cellular behaviour. Our microfluidic system offers a robust platform for high throughput studies that aim to understand combinatorial effects of multiple biochemical and microenvironmental factors.

Introduction

Tumour development is a very complicated process, exhibiting a vital relationship with the tumour's *in vivo* microenvironment.[1] The extracellular matrix (ECM) provides mechanical support and spatiotemporally regulated biochemical signals, guiding cancer cell proliferation, differentiation, migration, and apoptosis.[2–4] Therefore, constructing an *in vitro* ECM structure that closely mimics real tissue is very important for the precise study of cancer development.[5,6]

Invasion of the ECM by cancer cells is the first step in cancer metastasis. In order to realize distant metastasis, carcinoma cells must breach the barriers of the basement membrane, allowing them to invade the lymphatic vessels or blood vessels located within the neighboring collagen.[1] Although penetration of the basement membrane is a distinct clinical indicator of metastasis, it has to be noted that the barrier before the basement membrane is an epithelial layer, which is essential for basement membrane secretion and assembly.[7] Maintaining the integrity of the epithelial layer is therefore a means of avoiding metastasis by confining cancer cells to their primary site.

[a] *Beijing National Laboratory for Condensed Matter Physics and CAS Key Laboratory of Soft Matter Physics, Institute of Physics, Chinese Academy of Sciences, Beijing 100190, China. E-mail: fye@iphy.ac.cn*
[b] *College of Physics, Chongqing University, Chongqing 401331, China. E-mail: lyliu@cqu.edu.cn*
[c] *Materials Science and Engineering, Arizona State University, Tempe, Arizona, 85281 USA*
[d] *Division of Physical Science and Engineering, King Abdullah University of Science & Technology, Thuwal, 23955-6900 Saudi Arabia*
[e] *CAS Key Laboratory of Theoretical Physics, Institute of Theoretical Physics, Chinese Academy of Sciences, Beijing 100190, China. E-mail: oy@itp.ac.cn*
[f] *Key Laboratory of Optoelectronic Devices and Systems of Ministry of Education and Guangdong Province, Shenzhen University, Shenzhen, 518060 China*
[g] *Key Laboratory of Carcinogenesis and Translational Research (Ministry of Education), Department of Biobank, Peking University Cancer Hospital & Institute, Beijing 100142, P.R. China*
[h] *Key Laboratory of Carcinogenesis and Translational Research (Ministry of Education), Department of Thoracic Surgery II, Peking University Cancer Hospital & Institute, Beijing 100142, P.R. China*
[i] *School of Physical Sciences, University of Chinese Academy of Sciences, Beijing 100049, China*

† Electronic supplementary information (ESI) available. See DOI: 10.1039/c7lc00191f

How tumour cells interact with normal epithelial cells is still not fully understood, in part due to the lack of a realistic *in vitro* model. In traditional two-dimensional (2-D) cultures, cells can only attach to the floor of a Petri dish, and cannot form any 3-D structure; as such, the formation of the epithelial layer cannot be studied, not to mention the interference of cancer cells with the epithelial layer.[8,9] On the low adhesion surface (LAS) of 2-D culture systems, epithelial cells can aggregate into 3-D structures, but cultures of normal epithelial cells, as well as normal/cancer co-cultures, assemble into spheroids rather than lumina, which are the structure of epithelial layers *in vivo*.[10,11] There are also many other studies showing that *in vitro* cell cultures in 3-D are qualitatively different from 2-D Petri-dish cultures.[12,13] A 3-D environment can be emulated by embedding cells, cell clusters, or organoids in a biological hydrogel; however, structures that form are still qualitatively different from those of *in vivo* tissues, and many phenomena cannot be observed and further be studied.[14,15] For example, epithelial cells directly embedded in a low density Matrigel can form lumina similar to those in the *in vivo* epithelial layer.[16] However, *in vivo*, the hollow centres of the lumina provide spaces for the proliferation of cancer cells, which derived from the normal epithelial cell and proliferated into the lumen of the breast gland, then finally break through the lumina to be metastatic; *in vitro*, the lumina are filled with Matrigel, without the empty space for cancer cells, preventing the precise study of this phenomenon.

In order to better study processes such as the disruption of the epithelial layer by malignant cancer cells, we combine micro-moulding and microfluidic techniques to construct a 3-D microfluidic system with an array of collagen microchambers (MSACM). As shown in Fig. 1, the hollow microchambers in collagen are intended to mimic the spatial structure of hollow mammary glands, given that collagen I is the major component of the ECM in breast tissue. Meanwhile, the integrated microfluidic system allows construction of a controllable microenvironment,[17] such as the complex biochemical gradients around the collagen platform (Fig. 1A).[16,18] Collagen I is very soft, comprising 99% water and 1% gel, making it difficult to fabricate microstructures on collagen, especially when it is integrated into a small scale microfluidic system.[19] However, designing an *in vitro* system with collagen I has many advantages for mimicking the *in vivo* environment since collagen is one of the major components of ECMs, and is also a thick barrier for cancer cells before they reach the blood and lymphatic vessels and start metastasis.[20,21] The gradients of various factors, such as nutrition, oxygen, and anti-cancer drugs surrounding the tumour are also important to consider.[22] Molecular concentration gradients play an important role in biological phenomena such as chemotaxis, morphogenesis, and hypoxia.[23] In recent studies, drug gradients have also played a very important role in the emergence of resistance to chemotherapy for cancer.[23,24] The microfluidic system integrated into the MSACM assembly has been accomplished in this study to form delicately controlled complex gradients allowing for up to four biochemical gradients to exist at the same time.

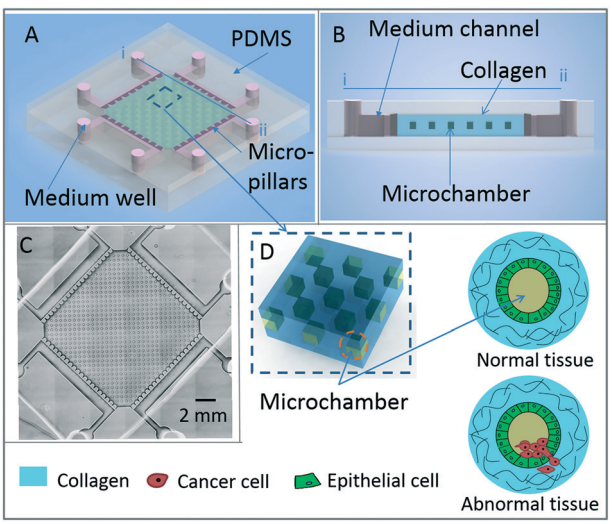

Fig. 1 The 3-D microfluidic system array of collagen microchambers (MSACM). (A) 3-D schematics of the MSACM model. (B) Cross-section view of the MSACM assembly. (C) Overview of the microfluidic chip. This microscopy image was taken in a bright field and processed with ImageJ. (D) Enlarged image shows the hollow microchamber within collagen, which partially mimicked the hollow structure of mammary glands.

We demonstrate that the MSACM system provides an environment in which MCF-10A epithelial cells can self-assemble into hollow, empty lumen-like structures. Further, we show that no aggregation is observed if the MCF-10A cells are co-cultured with MDA-MB-231 cancer cells, which we attribute to the E-cadherin expressed on the MCF-10A cell membrane which was cleaved by cancer cell MDA-MB-231 secreted MMPs. We find that when MMP inhibitors are added to the MCF-10A/MDA-MB-231 co-culture system at an appropriate concentration, MCF-10A cells can aggregate partially, but no lumen-like structures are formed. We also investigate co-culture systems of MCF-10A and MCF-7 (an epithelial phenotype breast cancer cell line), with the corresponding results presented in Fig. S1 of the ESI.†

Experimental

Cell culture

Normal human breast epithelial cell line MCF-10A marked with green fluorescent protein (GFP), and malignant breast cancer cell line MDA-MB-231 marked with red fluorescent protein (RFP) were obtained from China Infrastructure of Cell Line Resources (Beijing, China). MCF-10A-GFP cells were cultured in Dulbecco's modified Eagle's medium–F12 (DMEM/F12, Corning) supplemented with 5% horse serum (Gibco), 1% penicillin/streptomycin (Corning), 20 ng ml^{-1} human EGF (Gibco), 10 μg ml^{-1} insulin (Roche Diagnostics Gmbh), 100 ng ml^{-1} cholera toxin (Sigma), and 0.5 μg ml^{-1} hydrocortisone (Corning). MDA-MB-231-RFP cells were maintained in DMEM (Corning) supplemented with 10% fetal bovine serum

(Gibco) and 1% penicillin/streptomycin. All cells were cultured in an incubator at 37 °C with 5% CO_2.

In the co-culture experiments, MCF-10A-GFP and MDA-MB-231-RFP cells were seeded together in a 1 : 1 ratio, with a seeding cell density of 5×10^6 ml^{-1} for each type of cell. Cells were cultured in a 1 : 1 mixture of MCF-10A and MDA-MB-231 media.

Fabrication of the 3-D complex microfluidic system

A polydimethylsiloxane (PDMS) microfluidic chip is used to confine the collagen platform and to form a controllable microenvironment for cell culture, allowing the construction of multiple complex gradients *via* the independent microchannels surrounding the collagen platform. As Fig. 1A shows, there are four independent microchannels in the PDMS substrate, encompassing the central collagen platform. The collagen and the microchannels were separated by micropillars at the sides of the collagen platform. With this design, the medium in the microchannels can permeate into the collagen. The four microchannels were all independent and so the media in each channel did not mix. Since collagen has a porous structure, biochemical molecules can permeate through it slowly; if the media on different sides of the microchamber have differing concentrations of the molecules, the collagen platform can act as a buffer zone, and a concentration gradient forms across it.

The PDMS chip was designed with the L-Edit software (Tanner EDA). The designs were then printed onto a 5 inch chrome mask at high precision using a laser writer (Heidelberg DWL2000 Mask Writer). 4 inch p-type <100> silicon wafers with resistivity in the range 1–20 Ω cm and a thickness of 500 μm were cleaned and then spin-coated with positive photoresist with a thickness of 4.0 μm (ECL3027). The photoresist pattern was created by standard UV lithography techniques. After development, the silicon was put inside the RIE chamber (Reactive Ion Etching, Plasmalab System 100) with O_2 plasma to remove the residual photoresist on the exposed silicon regions (outside the photoresist pattern). The DRIE (Deep Reactive Ion Etching, Plasmalab System 100) Bosch process was then utilized to etch the exposed silicon regions down to 250 μm. After etching, the photoresist was removed with acetone and then the whole substrate was finally cleaned with a Piranha solution ($H_2SO_4 : H_2O_2 = 3 : 1$).

A Sylgard gel and elastomer (Dow Corning) were blended at a ratio of 10 : 1 and then the mixture was poured onto the fabricated silicon wafer to degas and gelled as PDMS.[25] As Fig. 2B shows, all fabricated PDMS pieces were peeled off the silicon wafer and sterilized with 75% ethanol before using. After drying, the feature surface of the PDMS substrate was incubated with 1 mg ml^{-1} poly-D-lysine (PDL) solution (Sigma) at 37 °C for 12 hours to enhance its adhesion to collagen. After incubation, the PDL solution was removed. The coated surface was rinsed thoroughly with sterile deionized water at least three times, and air-dried completely. A PDMS stamp with pre-defined microchamber features was covered

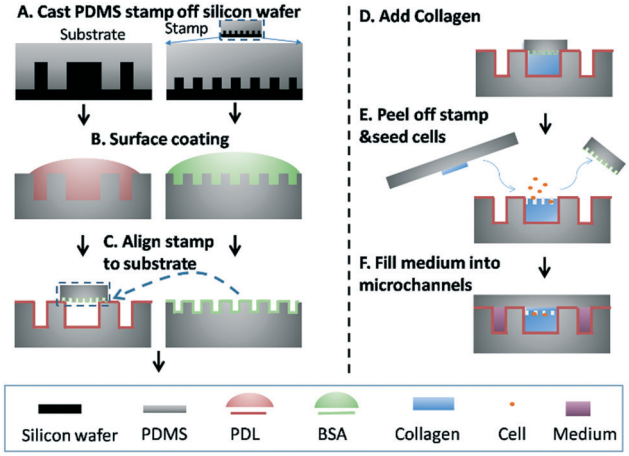

Fig. 2 Fabrication process for the MSACM assembly. (A) PDMS substrate and stamp was cast from the silicon wafer mould. (B) PDMS substrate surface was coated with PDL to enhance the adhesion to collagen, while the PDMS stamp surface was coated with BSA to help peel off the stamp from collagen. (C) PDMS stamp was aligned and covered to the PDMS substrate, forming a mould for collagen. (D) Collagen was injected into the chip and gelled. (E) PDMS stamp was unmoulded from the collagen. Cells were seeded into the formed microchambers on the collagen surface. Then the chip and collagen microchambers were covered with a cover glass, which was pre-coated with another layer of gelled thin flat collagen. (F) The microfluidic system was sealed by mechanical pressure. Medium was injected into the microchannels for future cell cultures.

with 2% bovine serum albumin (BSA, Beyotime) solution and left at room temperature for 30 min. The excess BSA solution was discarded, and the surface of the PDMS stamp was rinsed with sterile deionized water (pH 7.5) twice and pure water once to neutralize the remaining BSA solution. The coated stamp was purged with nitrogen to completely remove moisture. The BSA coating prevents the stamp from sticking to the collagen gel. The treated PDMS stamp was then aligned with the PDMS substrate bearing the microchannels, forming a mould for the collagen microchambers. Meanwhile, type I collagen (high concentration, 354249, Corning) stock solution was diluted and neutralized to 6 mg mL^{-1} with buffer solutions of 10× PBS (Corning), sterile deionized water, and 1 mol L^{-1} NaOH (Fluka). All dilutions were conducted on ice. The ice-cold liquid collagen was gently injected into the prepared PDMS mould through the pre-drilled collagen inlet in the PDMS substrate. Meanwhile, a thin layer of collagen was prepared by evenly spreading liquid collagen on a 30 × 30 mm cover glass, which served as the chip bottom to seal the collagen microchambers. Then both the collagen layers were heated at 37 °C for 1 hour to induce cross-linking. During the gelling process, the collagen layers were sealed in a Petri dish with pure water to prevent the collagen from drying. After the collagen had gelled, the PDMS stamp was carefully peeled off the PDMS substrate.[26]

The assembled chip was sealed by clamping with Plexiglas jigs (Fig. S2 in the ESI†). The top of the Plexiglas jig has eight medium wells, aligned with the medium inlets in the PDMS

substrate. Hollow windows in the centers of the top and bottom of the jig, at the position of the collagen platform, provided an observation window.

Cell seeding and experiments

A concentrated single cell suspension with a density of 5×10^6 ml^{-1} was prepared immediately before the experiment. In the co-culture system, the two types of cells were mixed together before seeding. The prepared cell suspension was kept on ice for 3–5 min to avoid sticking to the collagen. 20 μl of the cell suspension was added to collagen platform. After allowing two minutes of sedimentation of the cells into the micro chambers, excess cells outside the microchambers were rinsed off using a gentle and cold 1× PBS flow (flow rate 200 μl min^{-1}), while the cells in the microchambers were kept in place. The cell-seeded chip was then incubated at 37 °C for 15 min to allow the cells to stick firmly to the collagen. The gelled thin layer of collagen covered the microchambers, and the assembled chip was sealed with a Plexiglas jig. Finally, the culture medium was added to the chip.

Quantification of epithelial cell aggregation

To quantify the degree of lumen formation, we employ sensitive statistical morphological descriptors (*e.g.*, spatial correlation functions) derived from heterogeneous material theory.[27] Specifically, the fluorescence images of the cells were analysed and transformed to a two-phase (binary) image under a pre-set threshold intensity, which preserved the original cell clustering pattern. The two-point correlation function (eqn (2)) is then computed from the binary image for pattern quantification, as described in detail below.

Consider a two-phase texture in which phase i has a volume fraction ϕ_i (i = 1, 2) and is characterized by the indicator function

$$I^{(i)}(x) = \begin{cases} 1, & x \in V_i, \\ 0, & \text{otherwise}, \end{cases} \quad (1)$$

where V_i is the region occupied by phase i (equal to 1 or 2).

The standard two-point correlation function is defined as

$$S_2^{(i)}(x_1,x_2) = \langle I^{(i)}(x_1) I^{(i)}(x_2) \rangle = S_2^{(i)}(|x_1 - x_2|), \quad (2)$$

where the angular brackets indicate an ensemble average. This function is the probability of finding two points x_1 and x_2 both in phase i. Henceforth, we will drop the superscript "i" and only consider the correlation functions for the phase of interest (*i.e.*, the cell clustering patterns). For statistically homogeneous and isotropic patterns, the two-point correlation functions only depend on the distance $r \equiv |x_1 - x_2|$ between the points and hence $S_2(x_1,x_2) = S_2(r)$. The value of S_2 at a specific distance r indicates the degree of spatial correlation between two randomly selected points separated by a distance r, and thus, reflects the morphology of the pattern. For $r = 0$, S_2 provides the covering fraction of the cell clustering pattern φ; for large r values, S_2 approaches its asymptotic value φ^2.

S_2 was computed from the binary images of cell clustering patterns and normalized with respect to ϕ in order to highlight the spatial correlation information, *i.e.*,

$$S_2 = (S_2 - \varphi^2)/(\varphi - \varphi^2) \quad (3)$$

The normalized correlation functions are subsequently plotted and analysed. For lumen-like clustering patterns, the associated S_2 possesses large values for intermediate distances, indicating a high degree of spatial correlation. Such distances characterize the average linear size of the lumen. In contrast, if cells remain as small, isolated clusters, the S_2 value drops rapidly to the lowest value beyond a distance characterizing the average linear size of individual cells.

Immunofluorescence test

Certain important proteins need to be targeted and quantified in mechanism studies; this can be achieved with immuno-fluorescence tests.[28] At the stage when the microfluidic chip needed to be observed, 4% paraformaldehyde solution pre-warmed at 37 °C was added into the medium channel of the device for 1 hour to fix the biological sample. Then the sample was washed with 1× PBS three times to remove the paraformaldehyde solution. PBS was kept in chip for 30 min for each wash. Then the sample was incubated for 50 min in a blocking solution, consisting of 2% BSA in 1× PBS. After an extra wash with PBS, the sample was incubated with primary antibodies overnight at 4 °C. The primary antibody is 10 μg ml^{-1} anti-Ecadherin (Life Technology) in 0.1% BSA/PBS. Again the sample was washed three times with PBS, and then incubated with 1 : 125 diluted secondary antibodies (anti-mouse IgG (H + L), Alexa Fluor 647 Conjugate, CST4410) at 4 °C for 16 hours. Before imaging, the sample was rinsed with 1× PBS three times.

The immunofluorescence results were imaged by confocal laser scanning microscopy (CLSM), with a 25× water immersion objective. Sequential scanning was employed to minimize the interference from the different fluorescence channels. All the imaging parameters were kept constant for consistency in the subsequent semi-quantification of molecular expression. The fluorescence images were processed and analysed with the ImageJ software package.[29]

Results and discussion

Demonstration of complex gradient in the MSACM assembly

The ability to construct a gradient in a 3-D biochip, especially complex gradients for multiple molecules at the same time, is a very important advantage in an *in vitro* model. Spatial gradients in the microenvironment of the cells provide crucial signals for cell behaviours.

To our knowledge, the MSACM system is the first *in vitro* microenvironment that allows incorporation of multiple chemical, temporal, and spatial gradients within a micro-

patterned 3-D collagen system. The microfluidic chip has four independent microchannels surrounding the collagen platform, allowing up to four biochemical gradients simultaneously.

In the demonstration test, shown in Fig. 3A, 10 kDa red fluorescent Rhodamine–Dextran (Life Technology) solution was injected into the upper microchannel, green fluorescent 3 kDa FITC–Dextran (Life Technology) solution into left channel, and blue fluorescent Cascade blue–Dextran (Life Technology) solution into bottom channel. No fluorescent dye was injected into the right channel. All the dye solutions were prepared in 1× PBS at a concentration of 100 μg ml^{-1}. The solutions in the microfluidics system were refreshed every 12 hours to maintain a relatively constant concentration at the source and the sink. The chip was kept in an on-stage incubator, and observed under an inverted fluorescent microscope. Time-lapse fluorescence images were taken once an hour for 48 hours. Since the collagen platform area is 10 × 10 mm large, which is too far beyond the maximum field-of-view of the camera used in this study, a 4 × 4 image array was captured and stitched together to show the complete collagen area. The stitching trace appears as shadows at the edges of each small image.

Images for each of the three fluorescent molecules were taken and combined with ImageJ to examine the complex gradients (Fig. 3A). The images indicate that the complex gradients were all well-formed and stable. The gradients for each type of molecule were quantified by measuring the average fluorescence intensities of a series of 50 × 50 μm boxes at different positions along the central line, as indicated by dashed arrows in Fig. 3A. The statistical data were plotted as a 3-D surface map in Fig. 3B–D, showing the relative intensity distribution against the distance to the source channel as a function of time. The results for each molecular concentration gradient demonstrate that the complex gradient was stably formed at the collagen platform area. As indicated by Fig. 3B–D, the complex gradient for each colour can all be well maintained within the demonstration duration of at least 48 hours; technically speaking, the porous collagen platform can maintain the gradient stably as long as the media keeps constantly changing (a 2D version of Fig. 3C is presented in Fig. S3 in the ESI† to show the concentration change with time more clearly). Even though the fluorescence intensities next to the source microchannel experience occasional fluctuations as time passed, due to the patch refreshing flow every 12 hours, the gradient in the collagen buffer zone was stable, providing a very safe and stably buffered gradient area for cell cultures and all other kinds of gradient tests.

Since the MSACM system supports complex gradients in flexible combinations and with controllable concentrations, it is ideally suited for applications in research areas such as drug screening, chemoattractant, and cancer resistance.

The effect of MDA-MB-231 cancer cells on the aggregation of MCF-10A cells

As a benign tumour cell line, MCF-10A cells can express myoepithelial markers, such as the vimentin, alpha smooth muscle actin (SMA), CK5, CK17, and the basal-cadherin N-cadherin.[30] Thus the MCF-10A cell line is a widely used *in vitro* model for studying normal/benign breast cell functions and transformations.[9,31] In our experiments, MCF-10A-GFP or breast cancer cells MDA-MB-231-RFP were seeded and cultured in an MSACM assembly. As shown in Fig. 4A, most

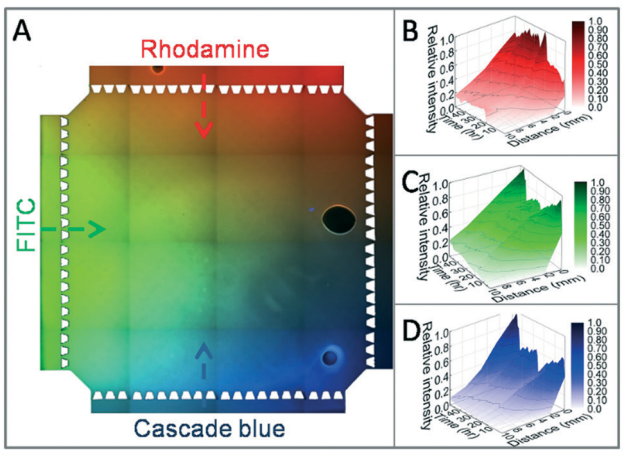

Fig. 3 Complex gradient demonstration with three types of fluorescent molecules. (A) Overview of the complex gradients. The image was the combination of three fluorescent channels. Stitching trace appears as shadows at the edges of each small image. (B) The statistical data of the Rhodamine–Dextran concentration gradient as the time-lapse result. (C) The statistical data of the FITC–Dextran concentration gradient as the time-lapse result. (D) The statistical data of the Cascade blue–Dextran concentration gradient as the time-lapse result.

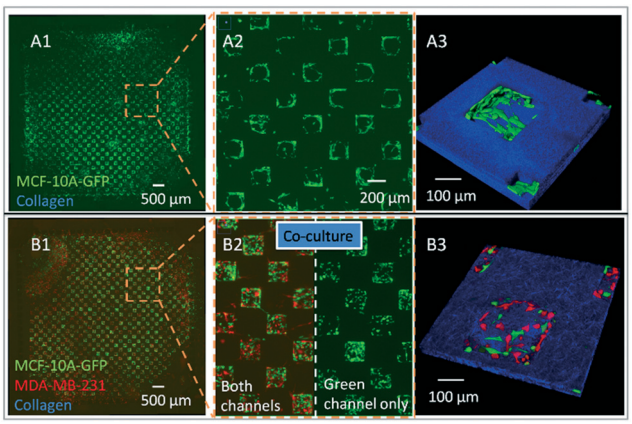

Fig. 4 Cell culture and morphology in microchambers within collagen. (A) MCF-10A-GFP mono-culture system. (B) MCF-10A-GFP and MDA-MB-231-RFP co-culture system. (A1 and B1) Overview of the microchambers on the whole collagen platform. (A2 and B2) Enlarged images showing part of the microchambers array. MCF-10A cells formed lumen structures in the mono-culture, while remained dispersed single cells in the co-culture system. (A3 and B3) Confocal images showing the cell distribution in a single microchamber. Collagen fibres were observed in reflection mode and displayed as blue.

cells were confined to the microchambers, although a few cells were left around the microchamber after rinsing. In the mono-culture system, MCF-10A cells gathered along the microchamber wall and formed lumen-like structures. As shown in Fig. 4A1, the whole chip comprises hundreds of microchambers. The enlarged view (Fig. 4A2) shows the structure formed in each microchamber. Collagen I fibres surrounding the microchambers can be imaged by CLSM in reflection mode. Fig. 4A3 shows that the MCF-10A cells gathered along the microchamber walls and attached to the collagen surface. This structure is very similar to that of which epithelial cells form *in vivo*, consisting of a ring of cells, 2–3 cells thick, with an empty central space. To our knowledge, this is the first time such a structure has been observed to form in an *in vitro* experiment.

The time-lapse images of MCF-10A cell aggregation (Fig. S4†) indicate that once seeded in the microchamber, MCF-10A cells spread out in the collagen chamber, forming small clusters as cells stick to each other (~2 h). These clusters move toward the chamber edges, forming lumen-like structures (<8 h). Once formed, these structures are dynamically stable for the remainder of the experiment, occasionally exchanging with cells in their surroundings.

We now employ a two-point correlation function to quantify the degree of aggregation of MCF-10A cells in the different systems. As shown in Fig. 5A, the inset images show the fluorescence images of cell clustering patterns from randomly selected microchambers from different locations of the chip. Each chamber was monitored for at least 3 days. The S_2 curves shown are the ensemble-averaged results of the cell distribution in different microchambers. In the MCF-10A cell mono-culture system, the MCF-10A cells were dispersed in the microchambers when they were just seeded at day 0. The associated S_2 drops rapidly and virtually goes to zero around distances of 40–60 μm, which indicates that the average cell cluster size is roughly 40 μm, consistent with the characteristic size of a spread single cell. In contrast, after one day, cells spread and aggregate, forming cell clusters, and there are a few isolated cells. The cell-cluster size in this case is much larger than the size of a single cell, indicating a long-ranged spatial correlation between cells. As shown in Fig. 5A, the S_2 value drops slowly with distance until ~140 μm for day 1 to day 3 curves. At this distance, the S_2 value reached its lowest, which indicates that the size of the cell-cluster formed is around 140 μm. The normalized S_2 curves of day 1 to day 3 are in good agreement, indicating that the MCF-10A cells can form the lumen-like aggregates in one day, which remain stable for at least three days.

In contrast, if the MCF-10A-GFP cells are co-cultured with malignant breast cancer cell MDA-MB-231-RFP at a ratio of 1 : 1, the formation of MCF-10A lumen structures was not observed. As shown in Fig. 4B, MCF-10A cells were dispersed randomly in the microchamber, without obvious aggregation. The time-lapse images (in Fig. S4†) show that in the co-culture system, MCF-10A cells often came into close contact, but these events didn't lead to cluster formation.

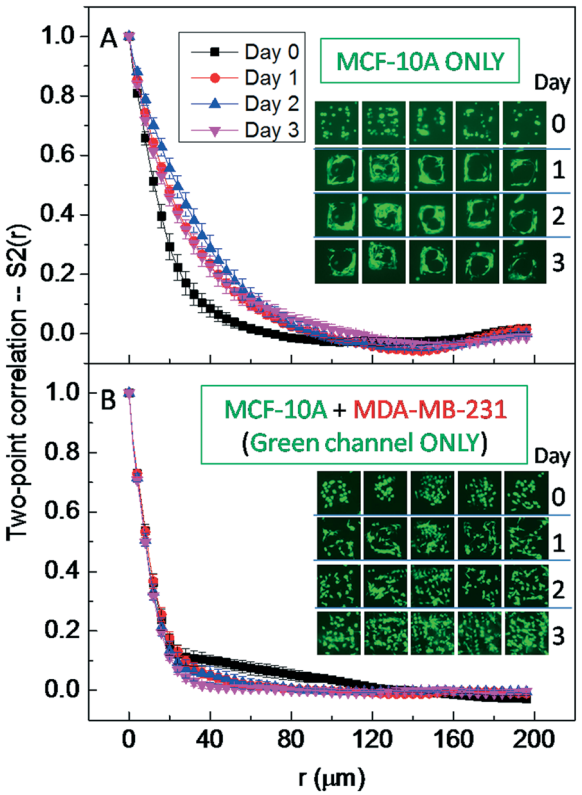

Fig. 5 Normalized two-point correlation (S_2) statistical data of the MCF-10A cell cluster in each microchamber *versus* the distance between two random points (r). (A) S_2 value of the MCF-10A mono-culture system. The slowly dropping S_2 value in day 1 to day 3, which reached the lowest level at around 140 μm, indicated that the large cell cluster formed in the mono-culture system at a size of around 140 μm. (B) S_2 value in the co-culture system. The rapidly dropping curves of day 1 to day 3, which were consistent with that of day 0, indicate that the MCF-10A cells remained in a single cell pattern in the co-culture system.

Fig. 5B shows the cell distribution for three days. From the associated S_2 curves, a rapid drop of S_2 as the distance increases can be clearly seen and S_2 decays to its asymptotic value beyond $r \sim 40$ μm for all data acquired from day 0 to day 3, which indicates that the MCF-10A cells always exist as dispersed single cells without forming any large clusters. The S_2 value of day 0 drops even much faster than those of the subsequent days, *i.e.*, with a correlation length of $r \sim 20$ μm. This is because on day 0, cells were just seeded and did not spread yet, which possessed a compact round shape and a small linear cell size. The inset images in Fig. 5B only show the MCF-10A-GFP cells (green channel), and hide the MDA-MB-231-RFP cells (red channel) in this co-culture system. The images show that though the MCF-10A cells also came into contact with each other, they didn't form tight connections and didn't aggregate together. The MCF-10A cells remained in a dispersed distribution in the following culturing days, until the microchamber was filled with cells, at which point it is difficult to distinguish the separate individual cells, since all cells appear to be in contact with their neighbours at such a high density.

This observation indicates that the malignant cell MDA-MB-231 can impede the aggregation of MCF-10A cells. This capability of MDA-MB-231 may assist its invasiveness by destroying the surrounding cell structures. The basement membrane which wraps the epithelial layer is considered to be a mechanical barrier to prevent malignant cells from invading the deeper ECM.[32] However, since the basement membrane is maintained by the epithelial layer, epithelial cells are the first barrier encountered by the malignant cells, other than the basement membrane.

Molecular mechanism and the function of MMP inhibitors

The reason MDA-MB-231 disrupts the formation of MCF-10A cell clusters is not yet clear. One of the most important molecules for the maintenance of the epithelial layer is Epithelial cadherin (E-cad), which is a transmembrane adhesion protein expressed by epithelial cells.[33] The extra-cellular domains of E-cad molecules from neighbouring cells bind to one another *via* a homotypic interaction. The intra-cellular domains of E-cad molecules bind to the actin cytoskeleton.[34] In this manner, E-cad forms adherens junctions that connect the actin cytoskeletons of neighbouring cells. Adherens junctions are the primary force-bearing junctions between epithelial cells.[35]

Matrix metalloproteinases (MMPs) are a group of proteases which can cleave the extracellular domain of membrane-bound E-cad at the aptly named MMP cleavage site. One important function of MMPs is to degrade extracellular matrix proteins. The secretion of MMPs is dramatically upregulated in invasive cancer cells and especially in the presence of collagen. MMPs can facilitate cell invasion by degrading the ECM surrounding cancer cells.[12,36,37] Therefore MMPs are very promising targets for anti-cancer-metastasis drugs.

In this report, a MMP inhibitor was employed to investigate the role of MMPs in inhibiting cell aggregation. To this end, the broad-spectrum MMP inhibitor batimastat (196440, Merck Millipore) was used. If the MMP expression of MDA-MB-231 cells was totally inhibited, E-cad expressed by the MCF-10A cells would not be down-regulated. A gradient of batimastat was applied to the MSACM assembly to mimic the *in vivo* situation, and to find out the appropriate batimastat concentration at one time. As shown in Fig. 6A, a cell culture medium with 40 μM batimastat, which was very high for inhibiting MMPs, was added to the left channel of the microfluidic chip once the co-cultured cells were seeded into the chip. Pure cell culture media were added to all the other three microchannels, without any batimastat. All media were refreshed every 12 hours during the cell culture period. Thus batimastat formed a concentration gradient along the direction indicated by the wide arrow as shown in Fig. 6A. The concentration of batimastat gradually decreased as the distance moves away from the batimastat medium channel (0–10 mm). Each microchamber in the collagen platform experienced a specific concentration at its position. Given that the MMP inhibitor does not have fluorescence emission for quantification, we then infer the concentration distribution of the MMP inhibitor from the aforementioned

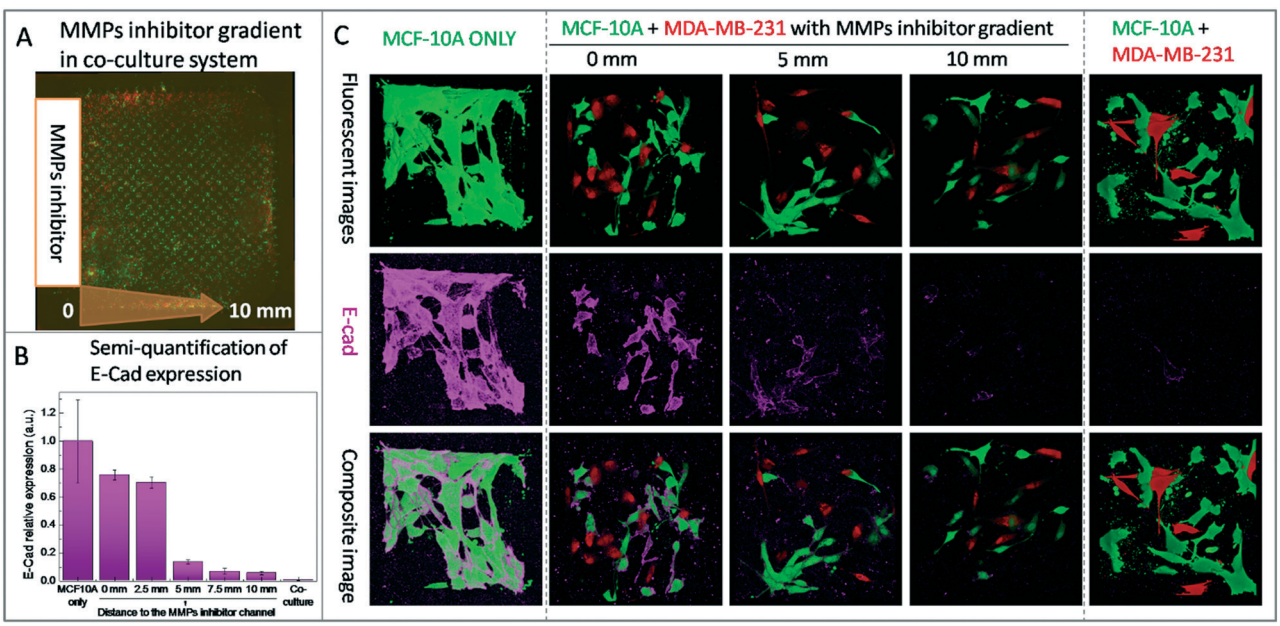

Fig. 6 The gradient of MMP inhibitor batimastat was applied in the 3-D MSACM system. (A) Overview of the microfluidic chip. The arrow indicated the concentration of batimastat from high to low. (B) Statistical data of relative E-cad expression *versus* the distance to the MMP inhibitor (batimastat) channel, showing that the relative values of E-cad expression (normalized to that of the MCF-10A monoculture group) on a chip with the batimastat gradient decrease from 0.758 ± 0.035 to 0.057 ± 0.014 as the chamber positions move away from the batimastat source microchannel and that in the co-culture system with no batimastat the value of the expression was only 0.007 ± 0.005. (C) Representative images of the cells' morphology and E-cad expression in single microchambers.

demonstration result of fluorescent molecules (see Fig. 3), by assuming that these two systems have similar diffusion patterns.

As the concentration of batimastat decreased along the gradient direction, the MMP inhibition effect on MDA-MB-231 was attenuated. Thus the MMPs secreted by MDA-MB-231 were actually increased, and E-cad expressed on MCF-10A cell membranes was down-regulated. The E-cad expression at different positions of the gradient was semi-quantified by immuno-fluorescence tests. Similar E-cad quantification was performed on control experiments without batimastat at all, which included the MCF-10A mono-culture system, and the co-culture system of MCF-10A and MDA-MB-231. For each chip, distances of 0, 2.5, 5, 7.5 and 10 μm away from the source channel, representing five levels of MMP inhibitor concentrations along the gradient, were chosen to characterize E-cad expression. For each distance, three microchambers distributed at different positions were analyzed to acquire the statistical E-cad expression. The image display and capture parameters were kept the same to guarantee the precision of the semi-quantification. Considering the cell size difference, in each chamber image, we normalized the E-cad expression (integrated intensity) to the total MCF-10A cell area instead of the cell number to obtain a good semi-quantification of the E-cad relative expression. As shown in Fig. 6B, the E-cad expression is the highest in the MCF-10A mono-culture system, and the lowest in the co-culture system with no batimastat; but with the presence of a batimastat gradient in the co-culture system, the E-cad expression gradually decreased, within the range between the highest and lowest values, as the concentration of batimastat decreased. Fig. 6C shows the representative images of the cells' morphology and E-cad expression in the single microchambers. In the MCF-10A mono-culture system, cell aggregation was dramatic. Cells fully spread and stick to each other; and the E-cad expression was also very high in all the cells. In the batimastat gradient of the co-culture system, as the distance from the batimastat channel (from 0 mm, 5 mm, to 10 mm) increased, the expression of MMPs was raised, and the E-cad expression decreased. In the presence of MMP inhibitors, though E-cad was up-regulated at a certain level, it was still not fully recovered to the normal level of no MDA-MB-231. In addition, probably due to the toxicity of batimastat to cells, the MCF-10A cells at the closest position to batimastat actually didn't show obvious aggregation, while the MCF-10A cells at the 5 mm position regained the most obvious aggregation, dramatic as that in the MCF-10A mono-culture system. In the co-culture system with no batimastat, the E-cad expression was the lowest, and the cells did not aggregate.

These data indicate that the MMP inhibitor batimastat can suppress the capabilities of the cancer cells to disrupt the structure of surrounding cell clusters, but the presence of batimastat cannot completely stop the cancer cells from destroying the lumen-like cell clusters. This is probably the reason why MMP inhibitors currently have many limitations in clinical applications. Other factors may be needed that co-operate with the MMP inhibitor in stopping cancer cell invasion; in this regard, the 3-D complex gradient microfluidic system can be utilized to combine various factors with MMP inhibitors for future studies.

Conclusions

In summary, a 3-D microfluidic system with an array of collagen microchambers (MSACM) was constructed, which combined the delicately controlled microenvironment (complex gradients) and 3-D cell culture microchambers within natural ECM materials (collagen). The MSACM is useful for biological studies, especially for cancer metastasis research, because it offers a well mimicked microenvironment with complex gradients and ECM structures to observe the interaction between cancer cells and the surrounding tissue components. The complex gradients within the MSACM also offer a high throughput screening technique to optimize the concentrations from combinations of various drugs and biochemical factors. Meanwhile, the transparency of the MSACM in optical microscopy makes it a powerful platform for real-time biological studies, such as migration within the hollow collagen chamber or invasion into collagen under a designed microenvironment. Furthermore, due to its reversibility, the sealed assembly can be opened up for picking out target cells with micro-manipulators for further biological analysis.

To demonstrate the advantages of the MSACM over 2D or simple 3D cell culture systems, we used it to study the *in vitro* behaviour of mono-culture epithelial cells (MCF-10A) and co-cultured systems of MCF-10A and cancer cells (MDA-MB-231). In the MSACM system, the mono-culture MCF-10A cells formed lumen-like structures on the wall of the microchambers within collagen. In contrast, if MCF-10A were co-cultured with cancer cells MDA-MB-231, the cancer cells impede the formation of lumen-like structure by MCF-10A cells, which indicates that the cancer cells have the ability to break their first barrier to start metastasis. In the immunofluorescence tests, the observation clearly shows that E-cad expression on MCF-10A cell membranes in the co-culture systems with cancer cell MDA-MB-231 was dramatically lower than that in the MCF-10A mono-culture systems. MMPs play an important role in this E-cad down regulation process. In the presence of an MMP inhibitor (batimastat) gradient, even co-cultured with cancer cells, the E-cad expression by MCF-10A was recovered in the chambers with high concentration of batimastat, while the E-cad expression was still kept at a very low level in the chambers with low batimastat concentration. This verifies that the ability of the cancer cells MDA-MB-231 to impede the formation of the surrounding lumen-like structure is strongly related to the function of secreted MMPs. It is, however, worthy to point out that real *in vivo* tissue structures are more complicated than the systems studied here; in the future, thin basement membrane layers and fibroblasts will be integrated into the model so as to even better mimic *in vivo* systems.

Acknowledgements

We thank Prof. Robert H. Austin in the Physics Department, Princeton University for stimulating discussions. This work was supported by the State Key Development Program for Basic Research of China (Grant No. 2013CB837200, No. 2013CB932803), the China Postdoctoral Science Foundation funded project (Grant No. 2016M591275), the Chinese Academy of Sciences, the Key Research Program of Frontier Sciences CAS (Grant No. QYZDJ-SSW-SYS014 and QYZDB-SSW-SYS003), the National Natural Science Foundation of China (Grant No. 11474345, No. 11674043, No. 11574382, the joint NSFC-ISF Research Program with Grant No. 51561145002), and Arizona State University start-up funds.

Notes and references

1 M. M. Shen, *Nature*, 2015, **520**, 298–299.
2 L. C. Kelley, L. L. Lohmer, E. J. Hagedorn and D. R. Sherwood, *J. Cell Biol.*, 2014, **204**, 291–302.
3 M. H. Lee, P. H. Wu, D. Gilkes, I. Aifuwa and D. Wirtz, *Oncotarget*, 2015, **6**, 32634–32645.
4 D. Wirtz, K. Konstantopoulos and P. C. Searson, *Nat. Rev. Cancer*, 2011, **11**, 512–522.
5 K. V. Nguyen-Ngoc, K. J. Cheung, A. Brenot, E. R. Shamir, R. S. Gray, W. C. Hines, P. Yaswen, Z. Werb and A. J. Ewald, *Proc. Natl. Acad. Sci. U. S. A.*, 2012, **109**, E2595–2604.
6 D. T. Butcher, T. Alliston and V. M. Weaver, *Nat. Rev. Cancer*, 2009, **9**, 108–122.
7 L. Smith, M. B. Watson, S. L. O'Kane, P. J. Drew, M. J. Lind and L. Cawkwell, *Mol. Cancer Ther.*, 2006, **5**, 2115–2120.
8 W. Q. Hu, Q. H. Fan and A. T. Ohta, *Lab Chip*, 2013, **13**, 2285–2291.
9 M. Nikkhah, J. S. Strobl, E. M. Schmelz, P. C. Roberts, H. Zhou and M. Agah, *Biomaterials*, 2011, **32**, 7625–7632.
10 W. Q. Hu, K. S. Ishii, Q. H. Fan and A. T. Ohta, *Lab Chip*, 2012, **12**, 3821–3826.
11 W. Song, C. K. Tung, Y. C. Lu, Y. Pardo, M. M. Wu, M. Das, D. I. Kao, S. B. Chen and M. L. Ma, *Soft Matter*, 2016, **12**, 5739–5746.
12 P. U. Patil, J. D'Ambrosio, L. J. Inge, R. W. Mason and A. K. Rajasekaran, *J. Cell Sci.*, 2015, **128**, 4366–4379.
13 K. Tanner and M. M. Gottesman, *Sci. Transl. Med.*, 2015, **7**, 283ps9.
14 J. B. Kim, *Semin. Cancer Biol.*, 2005, **15**, 365–377.
15 D. W. Hutmacher, *Nat. Mater.*, 2010, **9**, 90–93.
16 A. P. Wong, R. Perez-Castillejos, J. C. Love and G. M. Whitesides, *Biomaterials*, 2008, **29**, 1853–1861.
17 T. J. Liu, B. C. Lin and J. H. Qin, *Lab Chip*, 2010, **10**, 1671–1677.
18 B. J. Kim, P. Hannanta-anan, M. Chau, Y. S. Kim, M. A. Swartz and M. Wu, *PLoS One*, 2013, **8**, e68422.
19 M. D. Tang, A. P. Golden and J. Tien, *J. Am. Chem. Soc.*, 2003, **125**, 12988–12989.
20 B. M. Gillette, J. A. Jensen, B. Tang, G. J. Yang, A. Bazargan-Lari, M. Zhong and S. K. Sia, *Nat. Mater.*, 2008, **7**, 636–640.
21 X. Guan, *Acta Pharm. Sin. B*, 2015, **5**, 402–418.
22 A. Shamloo, N. Ma, M. M. Poo, L. L. Sohn and S. C. Heilshorn, *Lab Chip*, 2008, **8**, 1292–1299.
23 S. Sant, M. J. Hancock, J. P. Donnelly, D. Iyer and A. Khademhosseini, *Can. J. Chem. Eng.*, 2010, **88**, 899–911.
24 A. Wu, K. Loutherback, G. Lambert, L. Estevez-Salmeron, T. D. Tlsty, R. H. Austin and J. C. Sturm, *Proc. Natl. Acad. Sci. U. S. A.*, 2013, **110**, 16103–16108.
25 S. T. Keir, M. W. Dewhirst, J. P. Kirkpatrick, D. D. Bigner and I. Batinic-Haberle, *Anti-Cancer Agents Med. Chem.*, 2011, **11**, 202–212.
26 C. M. Nelson, J. L. Inman and M. J. Bissell, *Nat. Protoc.*, 2008, **3**, 674–678.
27 K. M. Connor, N. Hempel, K. K. Nelson, G. Dabiri, A. Gamarra, J. Belarmino, L. Van De Water, B. M. Mian and J. A. Melendez, *Cancer Res.*, 2007, **67**, 10260–10267.
28 V. V. Artym and K. Matsumoto, *Curr. Protoc. Cell Biol.*, 2010, **10**(18), 11–20.
29 M. McDermott, A. J. Eustace, S. Busschots, L. Breen, J. Crown, M. Clynes, N. O'Donovan and B. Stordal, *Front. Oncol.*, 2014, **4**, 40.
30 Y. Qu, B. C. Han, Y. Yu, W. W. Yao, S. Bose, B. Y. Karlan, A. E. Giuliano and X. J. Cui, *PLoS One*, 2015, **10**, e0131285.
31 M. H. Lee, P. H. Wu, J. R. Staunton, R. Ros, G. D. Longmore and D. Wirtz, *Biophys. J.*, 2012, **102**, 2731–2741.
32 L. Behrend, A. Mohr, T. Dick and R. M. Zwacka, *Mol. Cell. Biol.*, 2005, **25**, 7758–7769.
33 K. Woodson, J. A. Tangrea, T. A. Lehman, R. Modali, K. M. Taylor, K. Snyder, P. R. Taylor, J. Virtamo and D. Albanes, *Cancer Causes Control*, 2003, **14**, 513–518.
34 D. Robbins and Y. Zhao, *Antioxid. Redox Signaling*, 2014, **20**, 1628–1645.
35 Y. Kobayashi, K. Kariya, K. Saigenji and K. Nakamura, *Cancer Biother.*, 1994, **9**, 171–178.
36 D. Jiang, M. Sui, W. Zhong, Y. Huang and W. Fan, *Cancer Lett.*, 2013, **335**, 404–411.
37 C. L. Zhao, Y. L. Xie, Z. M. Mao, Y. H. Zhao, J. Rufo, S. K. Yang, F. Guo, J. D. Mai and T. J. Huang, *Lab Chip*, 2014, **14**, 384–391.